Extracellular Vesicle-Mediated Transfer of LncRNA *IGFL2-AS1* Confers Sunitinib Resistance in Renal Cell Carcinoma

Yihui Pan[1], Xuanxuan Lu[2], Guannan Shu[1], Junjie Cen[1], Jun Lu[1], Mi Zhou[3], Kangbo Huang[1,4], Jiaqi Dong[3], Jiaying Li[1], Haishan Lin[1], Hongde Song[1], Quanhui Xu[1], Hui Han[4], Zhenhua Chen[1], Wei Chen[1], Junhang Luo[1], Jinhuan Wei[1], and Jiaxing Zhang[3]

ABSTRACT

Sunitinib resistance remains a serious challenge to the treatment of advanced and metastatic renal cell carcinoma (RCC), yet the mechanisms underlying this resistance are not fully understood. Here, we report that the long noncoding RNA *IGFL2-AS1* is a driver of therapy resistance in RCC. *IGFL2-AS1* was highly upregulated in sunitinib-resistant RCC cells and was associated with poor prognosis in patients with clear cell RCC (ccRCC) who received sunitinib therapy. *IGFL2-AS1* enhanced TP53INP2 expression by competitively binding to hnRNPC, a multifunctional RNA-binding protein that posttranscriptionally suppresses TP53INP2 expression through alternative splicing. Upregulated TP53INP2 enhanced autophagy and ultimately led to sunitinib resistance. Meanwhile, *IGFL2-AS1* was packaged into extracellular vesicles through hnRNPC, thus transmitting sunitinib resistance to other cells. N^6-methyladenosine modification of *IGFL2-AS1* was critical for its interaction with hnRNPC. In a patient-derived xenograft model of sunitinib-resistant ccRCC, injection of chitosan-solid lipid nanoparticles containing antisense oligonucleotide-*IGFL2-AS1* successfully reversed sunitinib resistance. These findings indicate a novel molecular mechanism of sunitinib resistance in RCC and suggest that *IGFL2-AS1* may serve as a prognostic indicator and potential therapeutic target to overcome resistance.

Significance: Extracellular vesicle-packaged *IGFL2-AS1* promotes sunitinib resistance by regulating TP53INP2-triggered autophagy, implicating this lncRNA as a potential therapeutic target in renal cell carcinoma.

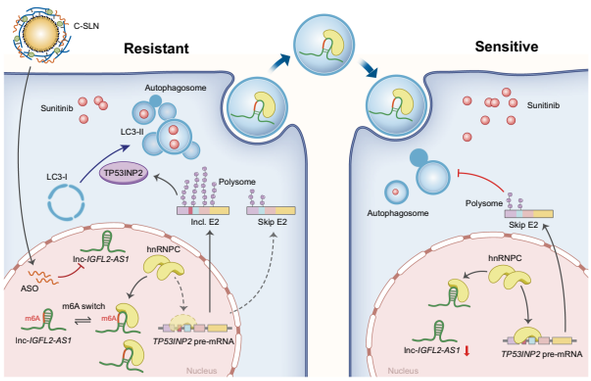

lnc-IGFL2-AS1, which can be transmitted via extracellular vesicles, promotes sunitinib resistance via control of alternative splicing and enhanced autophagy.

Introduction

In recent decades, the incidence of kidney cancer has continued to increase in both men and women throughout the world (1). Among patients with kidney cancer, approximately 85% are diagnosed with renal cell carcinoma (RCC), and 70% of RCC have a histology of clear cell RCC (ccRCC; ref. 2). Nearly 30% of all RCC cases include metastases at the time of first diagnosis (3). Moreover, one-third of patients with RCC treated with local resection have a relapse of their cancer at distant sites (4). Sunitinib is an oral multitarget receptor tyrosine kinase inhibitor (TKI), which can specifically inhibit the signaling pathways for vascular endothelial growth factor and platelet-derived growth factor receptor (5). As the representative of targeted therapies, sunitinib is still the recommended regimens for patients with metastatic ccRCC (mccRCC). However, approximately 60% to 70% of all patients with metastatic RCC exhibit inherent resistance to sunitinib therapy, and even responders can relapse after 11 months of therapy (6). Although previous studies have identified molecular markers of sunitinib efficiency *in vitro* (7, 8), the biological characteristics and underlying mechanisms of sunitinib resistance in mccRCC remain unclear.

Autophagy is a highly conserved self-degradation process in mammalian cells that maintains intracellular homeostasis, and has been reported to play an important role in tumorigenesis, tumor progression, and drug resistance (9). However, growing evidence has shown that this process may contribute to resistance to targeted therapies. Although excessive autophagy can exert cytotoxic effects that lead to autophagic cell death (10), drug resistance can also result from digestion of damaged organelles and proteins caused by targeted therapy and immunotherapy (11). Therefore, more studies are needed to explore these dual effects of autophagy on drug resistance.

[1]Department of Urology, First Affiliated Hospital, Sun Yat-sen University, Guangzhou, China. [2]Department of Food Science and Engineering, Jinan University, Guangzhou, China. [3]Department of Oncology, First Affiliated Hospital, Sun Yat-sen University, Guangzhou, China. [4]Department of Urology, Sun Yat-Sen University Cancer Center, Guangzhou, China.

Y. Pan, X. Lu, G. Shu, J. Cen, and J. Lu contributed equally to this article.

Corresponding Authors: Jiaxing Zhang, Department of Oncology, First Affiliated Hospital of Sun Yat-sen University, No. 58, Zhongshan Second Road, Guangzhou, Guangdong, 510000, China. E-mail: zhangjx25@mail.sysu.edu.cn; Jinhuan Wei, weijh23@mail.sysu.edu.cn; and Junhang Luo, luojunh@mail.sysu.edu.cn

Cancer Res 2023;83:103–16

doi: 10.1158/0008-5472.CAN-21-3432

This open access article is distributed under the Creative Commons Attribution-NonCommercial-NoDerivatives 4.0 International (CC BY-NC-ND 4.0) license.

©2022 The Authors; Published by the American Association for Cancer Research

Long noncoding RNAs (lncRNA) having a length of more than 200 nucleotides are one of the most diverse and abundant classes of ncRNAs (12). Generally, lncRNAs exert biological effects by regulating transcription, posttranscription, cellular organelles, and genome integrity (13). Accumulating evidence shows that lncRNAs are extensively involved in phenotypes associated with cancer, such as stemness, proliferation, invasion, and metastasis (14–17). Meanwhile, bioactive lncRNAs can be packaged into extracellular vesicles (EV) and transmitted to surrounding tumor cells (18, 19). However, a role of lncRNAs in sunitinib resistance has not been fully understood.

Herein, we constructed two acquired sunitinib-resistant RCC models and identified a novel lncRNA, insulin growth factor-like family member 2 antisense 1 (*IGFL2-AS1*), which is significantly overexpressed in sunitinib-resistant RCC cells. *IGFL2-AS1* enhanced tumor protein p53 inducible nuclear protein 2 (TP53INP2) expression by competitively binding to heterogeneous nuclear ribonucleoprotein C (hnRNPC), an RNA-binding protein that suppressed TP53INP2 expression through alternative splicing. Increased TP53INP2 promoted autophagy and thus led to sunitinib resistance in RCC cells. Furthermore, binding to hnRNPC allowed *IGFL2-AS1* to be packaged into EVs to transmit sunitinib resistance to other cells. In addition, N^6-methyladenosine (m^6A) modification in *IGFL2-AS1* was critical to its interaction with hnRNPC. On the basis of these findings, we developed a novel nanomedicine, chitosan-solid lipid nanoparticles (C-SLN), which could deliver antisense oligonucleotide (ASO)-*IGFL2-AS1* stably and efficiently for *in vivo* treatment of sunitinib-resistant ccRCC in a patient-derived xenograft (PDX) model.

Materials and Methods

Sunitinib-resistant RCC cell models and PDX models

For our sunitinib-resistant RCC cells xenograft mice model, 4 to 5 weeks old male BALB/c-Nu mice (RRID:IMSR_GPT:D000521) were housed and fed in specific pathogen free conditions. 786-O cells and ACHN cells were injected subcutaneously with a concentration of 5×10^6 cells/100 μL. The tumor volume was calculated as length × width × width/2 and measured weekly. When the tumor volume reached 200 mm^3, the first-generation mice were treated with sunitinib (40 mg/kg/day) or vehicles orally on the basis of a standard treatment schedule: 4 weeks on and 2 weeks off. Sunitinib was purchased from Selleck and dissolved in 5% DMSO + corn oil. Six weeks later, all the mice were sacrificed. Tumors were separated surgically and cut into 1 mm^3 tumor blocks. The mice of second generation were grafted with 1 mm^3 tumor blocks and followed with vehicle or sunitinib treatment. After the sacrifice of third generation mice, the isolated tumors were disaggregated surgically and washed with cold PBS containing 2% penicillin-streptomycin solution and levofloxacin (100 μg/mL). Then the tumors were digested in the DMEM medium containing 0.2% Collagenase 4, 0.01% Hyaluronidase and 0.002% DNase I (Stemcell) at 37°C for 45 minutes with continuous shaking. The cell suspension was centrifuged at 300 × *g* and the supernatant were plated in 6-well plate with a concentration of 7×10^5 cells/well. Fibroblasts were removed through the method of reduplicative adherence. Sunitinib-resistant RCC cells were named 786-O-R and ACHN-R, respectively.

To generate sunitinib-resistant RCC cells *in vitro*, 769-P cells were cultured with an increasing dose of sunitinib (2–10 μmol/L). Ten months later, a sunitinib-resistant cell line was obtained and named 769-P-R.

For our ccRCC PDX models, 4 to 5 weeks old male NCG (NOD/ShiLtJGpt-Prkdcem26Cd52Il2rgem26Cd22/Gpt) mice (IMSR, Catalog No. GPT_T001475, RRID:IMSR_GPT:T001475) were transplanted with the fragments of fresh human RCC tissues into flanks subcutaneously. The tumor volume was measured weekly. When the tumor volume reached 100 mm^3 (approximately 4 weeks), the mice were sacrificed. The tumors were cut into 1 mm^3 pieces and transplanted into the second-generation mice. After three generations, we obtained a stable ccRCC PDX model. We constructed seven ccRCC PDX models in total and chose the one with highest expression of *IGFL2-AS1* and highest IC_{50} value of sunitinib for the following experiments. For the orthotopic xenograft model, NCG mice were anesthetized with 1% pentobarbital (50 mg/kg body weight) in PBS. A piece of PDX tumor (1 mm^3) was transplanted into the right renal subcapsule orthotopically, and fixed with 3M Vetbond Tissue Adhesive. For the subcutaneous xenograft model, anesthetized NCG mice were transplanted with a piece of PDX tumor (1 mm^3) subcutaneously. During the oral gavage of sunitinib, PBS, C-SLN, ASO-*IGFL2-AS1*, or C-SLN/ASO-*IGFL2-AS1* were tail-vein injected to NCG mice for 4 weeks (5 nmol every 3 days). After 2 weeks off, all the mice were sacrificed and the tumors were disaggregated surgically for TUNEL assay or IHC stain.

All the animal studies were examined and approved by the Institutional Animal Care and Use of Sun Yat-sen University Cancer Center. The *in vivo* experiments were carried out in accordance with the guidelines for the care and use of animals.

Cell lines

The human RCC cell lines 786-O (RRID:CVCL_1051), 769-P (RRID:CVCL_1050), and ACHN (RRID:CVCL_1067) were purchased from the Cell Bank of the Chinese Academy of Sciences. The establishment of sunitinib-resistant RCC cell lines 786-O-R, ACHN-R, and 769-P-R were described in the "Sunitinib-resistant xenograft experiments and PDX models."

786-O cells, 786-O-R cells, 769-P cells, and 769-P-R cells were cultured in RPMI1640 medium (Gibco). ACHN cells and ACHN-R cells were cultured in DMEM medium (Gibco). Both media were supplemented with 10% FBS (PAN-Seratech) and 1% penicillin-streptomycin (Biosharp) at 37°C with 5% CO_2. 786-O, 769-P, and ACHN were examined with the short tandem repeat (STR) profiling by vendors. All cells were periodically tested for *Mycoplasma* infection.

ccRCC patient samples and follow-up data

This study was approved by the Institutional Review Board and Human Ethics Committee of Sun Yat-sen University Cancer Center and the First Affiliated Hospital, Sun Yat-Sen University. Written informed consent was signed by the participants and their surrogates for the use of human ccRCC tissue specimens and serum samples. At first, we collected successively a total of 82 patients with ccRCC treated with sunitinib between 2010 and 2018 from Sun Yat-sen University (SYSU). Patients were excluded if their samples were not taken before sunitinib therapy, or their follow-up data and laboratory examination information were incomplete, or RNA contents were less than 5 ng/μL. After initial screening, we retained 72 patients with ccRCC, including 14 patients from the First Affiliated Hospital, Sun Yat-Sen University and 58 patients from the Sun Yat-sen University Cancer Center (SYSUCC). All patients underwent nephrectomy before sunitinib therapy. All tested tissues were primary tumors. Out of 72 patients with ccRCC, serum samples from 60 patients with ccRCC were sufficient for EV extraction. All serum samples were obtained before sunitinib therapy. Both tumor tissues and serum-derived EVs were used for qRT-PCR analysis of *IGFL2-AS1*. The detailed clinical characteristics are provided in Supplementary Table S1 to S4. Tumor blocks used for PDXs were obtained in 2019 from the First Affiliated Hospital, Sun Yat-Sen University. The detailed clinical characteristics

were provided in Supplementary Table S5. All samples used in this study were approved by the Medical Ethics Committee of the First Affiliated Hospital, Sun Yat-sen University, and the Sun Yat-sen University Cancer Center. Progressive disease (PD) was defined as the appearance of new lesions, or a 20% increase in the sum of diameters of target lesions. Overall survival (OS) was defined as the time from initiation of sunitinib treatment to the date of death from any reason. Progression-free survival (PFS) was defined as the time from initiation of sunitinib treatment to the date of first radiologic evidence of PD.

RNA pull-down, silver staining, and MS analysis

RNA pull-down assay was performed using Pierce Magnetic RNA-Protein Pull-Down Kit (Thermo Fisher Scientific) according to manufacturer's instructions. The RNA probes were obtained using a T7 Transcription Kit (Invitrogen) and labeled with biotin with an RNA 3′ End Desthiobiotinylation Kit (Thermo Fisher Scientific) according to manufacturers' instructions. The protein samples were loaded in each lane of SDS-PAGE. After electrophoresis, the gel was stained with a Fast Silver Stain Kit (Beyotime). Targeted region of gel was cut off and saved in microcentrifuge tubes. MS analysis was provided by BGI.

FISH

The labeled *IGFL2-AS1* probes were synthesized from Umine Biotechnology. FISH was performed with Fluorescent In Situ Hybridization Kit (RiboBio) according to manufacturer's instructions. The images were obtained using OLYMPUS FV1000 confocal microscopy. The U6 and 18S probes were provided by RiboBio. The *IGFL2-AS1* probe sequence was shown as below:

IGFL2-AS1: 5′-Cy3 labeling-AGAACUCAUUCACCUGUCCUC-AGUUGUCUG GAAAUAGGCUUUUCUGGGAU-3′

RNA interference

All the siRNAs, ASOs, and corresponding negative controls were provided by RiboBio. siRNAs and ASOs were transfected into RCC cells using RNAiMAX (Invitrogen) according to manufacturers' instructions. Function tests were performed 48 hours after the transfection. Targeting sequences of siRNA and ASO were listed in Supplementary Table S6.

RNA immunoprecipitation

RNA immunoprecipitation (RIP) assay was carried out using an EZ-Magna RIP Kit (Millipore) according to manufacturer's instructions. The m^{6}A RIP assay was carried out using a Magna MeRIP m^{6}A Kit (Millipore) according to manufacturer's instructions. The rRNAs were removed from the total RNA before the specific enrichment. Five micrograms of IgG, anti-hnRNPC antibody (Santa Cruz Biotechnology, Catalog No. sc-32308, RRID:AB_627731) and anti-m^{6}A antibody (Synaptic Systems, Catalog No. 202 003, RRID:AB_2279214) were used for each sample. The precipitated RNAs were examined through qRT-PCR analyses. The specific primers used for qRT-PCR were presented in Supplementary Table S7.

EVs experiments

The blood sample was collected into clot activator tubes and incubated at room temperature for 30 minutes. After clotting, the blood sample was centrifuged at 1,880 × *g* for 10 minutes at room temperature. An equal volume of serum (2 mL) was collected and diluted with PBS. The diluted serum was then centrifuged at 300 × *g* for 10 minutes, 2,000 × *g* for 10 minutes, 10,000 × *g* for 30 minutes in turn. After filtration with a 0.22 μmol/L filter (Millipore), the filtrate was centrifuged at 120,000 × *g* for 70 minutes twice (Beckman Coulter). The pellets were resuspended with PBS and prepared for the following experiments.

RCC cells were grown in medium with 10% EV-depleted FBS (System Biosciences) for 72 hours before the isolation of EVs. The supernatant was collected and centrifuged at 300 × *g* for 10 minutes, 2,000 × *g* for 10 minutes, 10,000 × *g* for 30 minutes in turn. After filtration with a 0.22 μmol/L filter, the filtrate was centrifuged at 120,000 × *g* for 70 minutes twice. The pellets were resuspended with PBS and prepared for the following experiments.

The morphology of EVs was taken by JEM1200-EX TEM (JEOL). The size of EVs was detected by Nanosight ns300 (Malvern Instruments Ltd.). The EV protein markers were examined through Western blotting. The specific primary antibodies applied in this study were presented in Supplementary Table S8.

For qRT-PCR analyses of serum-derived EVs, synthesized λ polyA$^+$ RNA (Takara) was used as the external reference. Specifically, 1.8 × 10^8 λ polyA$^+$ RNAs were added to the EV suspension (normalized by volume of serum) before RNA extraction. For qRT-PCR analyses of CM-derived EVs, lncRNAs were normalized against λ polyA$^+$ RNAs per million EV particles. Specifically, 1.8 × 10^8 λ polyA$^+$ RNAs were added to the EV suspension before RNA extraction. The number of EV particles was quantified by NanoSight ns300, using NTA 3.0 software. The RNAs in EVs were extracted using an EV RNA Purification Kit (EZBioscience) according to manufacturer's instructions.

Polysome analysis

Before lysis, approximately 1.5 × 10^7 cells were incubated in complete RPMI1640/DMEM medium with 100 μg/mL cycloheximide (CHX) at 37°C for 10 minutes. The cells were collected and centrifuged for 5 minutes (1,000 × *g*, 4°C). After removing the supernatant, 500 μL lysis buffer [300 mmol/L NaCl, 20 mmol/L Tris-HCl pH 7.4, 10 mmol/L $MgCl_2$, 1% Triton X-100, 1 mmol/L 1,4-dithiothreitol, 100 μg/mL CHX, 0.5% (w/v) sodium deoxycholate, EDTA-free protease inhibitor cocktail, RNase inhibitor] were added and each sample were kept on ice for 10 minutes. Then the cleavage products were centrifuged for 5 minutes (13,000 × *g*, 4°C) and the supernatants were collected for RNA concentration measurements.

Gradient were made with 5% and 50% sucrose solution containing 100 μg/mL CHX in Gradient Master108 (Biocomp). Equal cell extracts were added to the top of each gradient in the ultracentrifuge tube (Beckman Coulter). Tubes were loaded in a SW41 rotor and centrifuged in Beckman Coulter OptimaTM L-100XP (Beckman Coulter) at 39,000 rpm for 120 minutes at 4°C. Twelve fractions were collected respectively from the ultracentrifuge tube using Piston Gradient Fractinator (Biocomp). RNA was extracted from each tube with TRIzol LS Reagent (Invitrogen). After reverse transcription, qRT-PCR analyses were performed to evaluated the distribution of *TP53INP2* in polysomes.

Bioinformatics analysis

The coding potential of *IGFL2-AS1* was evaluated through five methods in the LNCipedia database (20). The predicted sequence motif of hnRNPC binding site were obtained from POSTAR2 (21). The predicted secondary structure of *IGFL2-AS1* were downloaded from RNAalifold (http://rna.tbi.univie.ac.at/cgi-bin/RNAWebSuite/RNAfold.cgi). The m^{6}A modified sites in *IGFL2-AS1* were predicted based on RNA sequences and machine learning using SRAMP (22). The m^{6}A-seq data showing m^{6}A peaks of *IGFL2-AS1* were obtained

from REPIC (23). EV database Vesiclepedia was utilized to assess the distribution of hnRNPC in EVs (24).

Statistical analysis

All statistical analyses in this study were carried out using SPSS 25.0 software (RRID:SCR_002865) and GraphPad Prism 8.3.0 (RRID:SCR_002798). Mann–Whitney–Wilcoxon tests were used for comparisons between pairs of groups. For comparisons among three or more groups, Kruskal–Wallis tests with Bonferroni correction were applied. Pearson' Chi-square test was used to test association between *IGFL2-AS1* expression and clinical characteristics. OS and PFS were evaluated through Kaplan–Meier survival analysis and examined by the log-rank test. The median expression of *IGFL2-AS1* was set as the cutoff point for the low and high expression groups. Univariate and multivariate Cox regression analyses were performed to evaluate independent prognostic predictors. All *in vitro* experiments were repeated at least in triplicate unless otherwise indicated. Data were presented as mean ± SD. The statistical difference was confirmed when the P value < 0.05 (*, $P < 0.05$; **, $P < 0.01$; ***, $P < 0.001$).

Data availability statement

All data associated with this study are presented in the paper or the Supplementary Data. The materials that support the findings of this study are available from the corresponding author on reasonable request.

Results

Overexpression of lnc-*IGFL2-AS1* in sunitinib-resistant RCC cells

There is growing evidence for involvement of lncRNAs in tumor progression, metastasis, and drug resistance. To examine possible lncRNAs involved in sunitinib resistance in RCC, we constructed two sunitinib-resistant RCC cell lines *in vivo*, named 786-O-R and ACHN-R, and one sunitinib-resistant RCC cell line *in vitro*, named 769-P-R (**Fig. 1A**; Supplementary Fig. S1A). To examine the sunitinib resistance, we performed CCK8 assays, caspase 3/7 activity assays and flow cytometry (Supplementary Figs. S1B–S1G). Remarkably, 786-O-R, ACHN-R, and 769-P-R cells exhibited higher sunitinib resistance, higher IC_{50} values, lower caspase 3/7 activity, and lower apoptosis rates than parental cells when treated with sunitinib.

We next conducted a high-throughput RNA-sequencing (RNA-seq) to compare lncRNAs expressions between sunitinib-resistant and parental RCC cell lines. Kyoto Encyclopedia of Genes and Genomes (KEGG) analysis of the upregulated genes in resistant RCC cells showed enriched pathways, such as regulation of autophagy (**Fig. 1B**). To identify lncRNAs necessary for sunitinib resistance in RCC, we performed four rounds of screening (**Fig. 1C**). First, the heatmap showed the top 20 most increased or decreased lncRNAs among 297 differentially-expressed lncRNAs (fold change >3, $P < 0.001$; **Fig. 1D**). Second, among the top 20 differentially-expressed lncRNAs, seven lncRNAs in common amplified (chromosome 5q, 7, 19, and 22q) or deleted regions (chromosome 3p, 8p, and 14q) of RCCs were identified (25). Third, we validated the expression of 7 lncRNAs by qRT-PCR in parental and resistant RCC cells. Only *IGFL2-AS1* and *LINC01111* showed expression differences consistent with RNA-seq (Supplementary Fig. S2A). Finally, we conducted a combination of siRNA and ASO, and only interference of lncRNA *IGFL2-AS1* suppressed sunitinib resistance in sunitinib-resistant RCC cells (**Fig. 1E**; Supplementary Figs. S2B and S2C). Thus, we decided to concentrate on lnc-*IGFL2-AS1*. *IGFL2-AS1* is located on human chromosome 19 and consists of three exons (Supplementary Fig. S2D). The full length of *IGFL2-AS1* is 1686 nt as confirmed by the rapid amplification of cDNA ends (RACE) assay (**Fig. 1F**; Supplementary Figs. S2E and S2F). Northern blot analysis showed that expression of *IGFL2-AS1* in sunitinib-resistant RCC cells was higher than that in parental RCC cells (Supplementary Fig. S2G). The protein coding potential of *IGFL2-AS1* was ruled out by coding-potential analysis (Supplementary Fig. S2H). We conducted RNA-FISH and cellular fractionation analysis, confirming that *IGFL2-AS1* was mainly localized in the nuclei of RCC cells (**Fig. 1G**; Supplementary Fig. S2I).

To study whether lncRNA *IGFL2-AS1* was involved in clinical ccRCC progression, we first collected and analyzed expression of *IGFL2-AS1* in the SYSU cohort, where each patient with ccRCC endured relapse or metastasis after surgery and received sunitinib. Remarkably, prolonged OS and PFS were observed in the low *IGFL2-AS1* expression group (**Fig. 1H** and **I**; Supplementary Tables S1 and S2). These data showed that *IGFL2-AS1* might play an important role in the progression of ccRCC and serve as a potential prognostic biomarker for patients with metastatic ccRCC.

Loss or gain of function of *IGFL2-AS1* associated with sunitinib resistance

First, we examined and validated the sunitinib-resistant effect of *IGFL2-AS1 in vitro* through CCK8 assays, clone formation, and flow cytometry. Remarkably, *IGFL2-AS1* knockdown resulted in reduced cell viability, reduced numbers and sizes of colonies, and increased apoptosis in sunitinib-resistant RCC cells (**Fig. 2A**–**H**; Supplementary Figs. S3A–S3D). In contrast, *IGFL2-AS1* overexpression elicited the opposite response in RCC cells. Next, we constructed an *in vivo* tumor model to examine the effect of *IGFL2-AS1* (Supplementary Figs. S3E and S3F). Similarly, after sunitinib treatment, slower tumor growth, smaller tumor size, and lower tumor weight were observed in the *IGFL2-AS1* knockdown groups (**Fig. 2I** and **J**; Supplementary Fig. S3G). Meanwhile, *IGFL2-AS1* overexpression largely enhanced tumor growth and tumor weight when cells were treated with sunitinib (**Fig. 2K** and **L**; Supplementary Fig. S3H). TUNEL assay results were consistent with the results described above (**Fig. 2M**; Supplementary Fig. S3I).

IGFL2-AS1 overexpression enhances autophagy in RCC cells by regulating alternative splicing of *TP53INP2*

Extensive evidence supports a critical role for autophagy in tumor progression and drug resistance. However, its effect on sunitinib resistance in ccRCC remains unclear. According to the transcriptome KEGG analysis shown in **Fig. 1B**, we tested the key regulators of five tumor-related pathways with most significant changes ($P < 0.001$), including TNF signaling pathway, autophagy pathway, chemokine signaling pathway, PI3K-Akt signaling pathway, and Jak-STAT signaling pathway (**Fig. 3A**; Supplementary Fig. S4A). Remarkably, upon sunitinib treatment, we only observed a significantly higher LC3-II/LC3-I ratio in *IGFL2-AS1*-overexpressing group. Therefore, we determined to focus on autophagy pathway in RCC cells. It is well known that LC3 plays an important role in autophagy flux. Confocal microscopy of labeled LC3 showed enhanced autophagy in *IGFL2-AS1*-overexpressing RCC cells upon sunitinib treatment (**Fig. 3B**; Supplementary Fig. S4B). Consistently, electron microscopy also revealed increased numbers of autophagosomes/autolysosomes when overexpressing *IGFL2-AS1* in RCC cells treated with sunitinib (**Fig. 3C**). Next, we examined key regulators affecting the transition from LC3-I to LC3-II, including ATG3, ATG7, and TP53INP2, and found that the level of TP53INP2 protein significantly increased upon *IGFL2-AS1* overexpression (**Fig. 3D**). Consistently, the TP53INP2 protein level

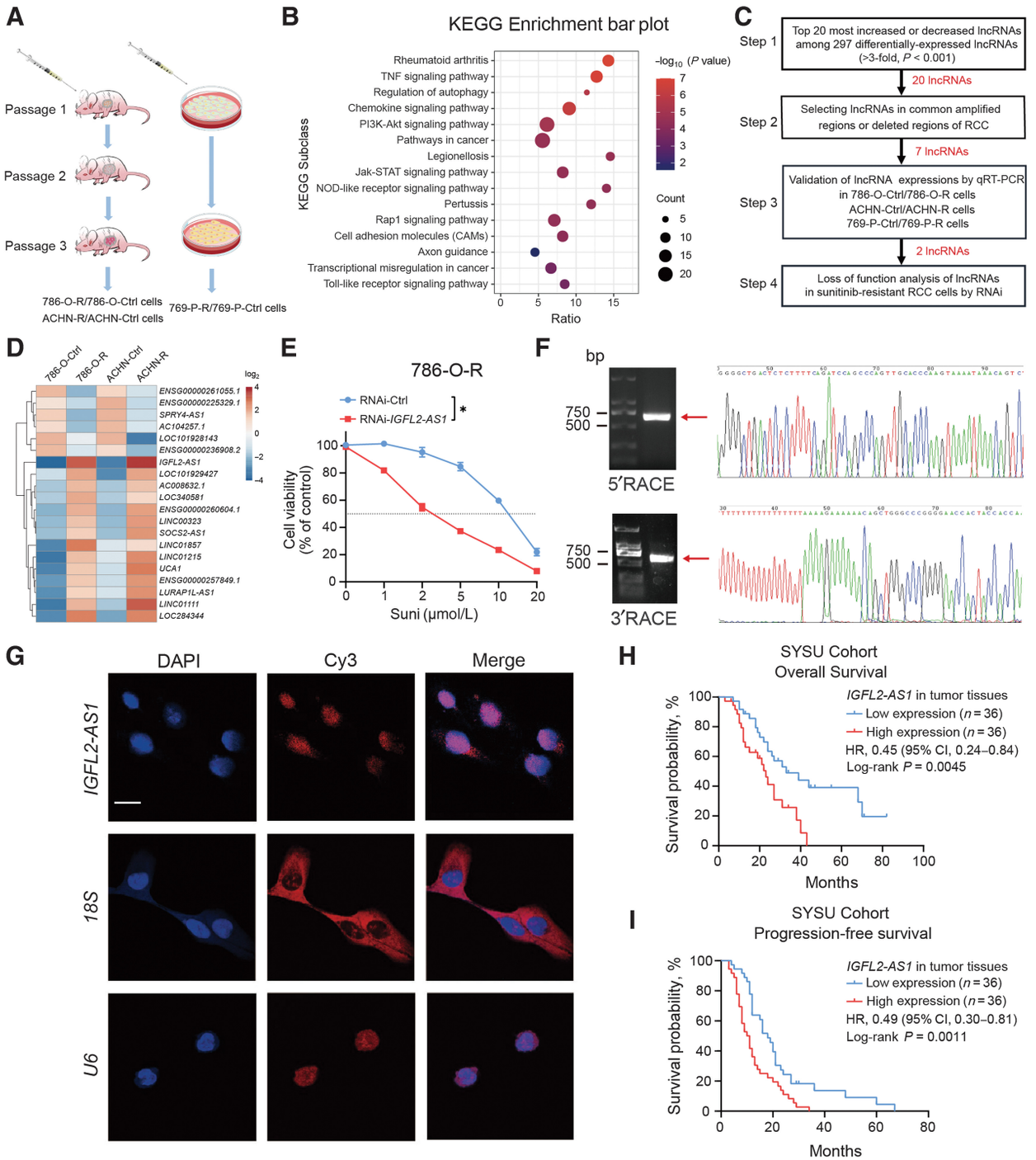

Figure 1.

lnc-*IGFL2-AS1* is highly expressed in sunitinib-resistant RCC cells and is associated with poor prognosis. **A,** Schematic illustration of the modeling process to obtain sunitinib-resistant RCC cells. **B,** KEGG analysis of the upregulated genes in resistant RCC cells by RNA-seq. **C,** Flow chart of screening differentially expressed lncRNAs identified by RNA-seq. **D,** Heatmap of top 20 most increased or decreased lncRNAs between sunitinib-resistant RCC cells and related parental RCC cells. **E,** Relative cell viability of 786-O-R calculated by CCK8. **F,** Representative image of agarose gel electrophoresis and Sanger sequencing of the 5′-RACE and 3′-RACE products of *IGFL2-AS1*. **G,** Intracellular localization of *IGFL2-AS1* was examined in RCC cell lines by RNA-FISH assays. White scale bar, 20 μm. **H** and **I,** Kaplan–Meier survival analysis for patients with ccRCC from the SYSU cohorts. CI, confidence interval. A *P*-value < 0.05 was considered as significant. Data are shown as mean ± SD (error bars). *, $P < 0.05$.

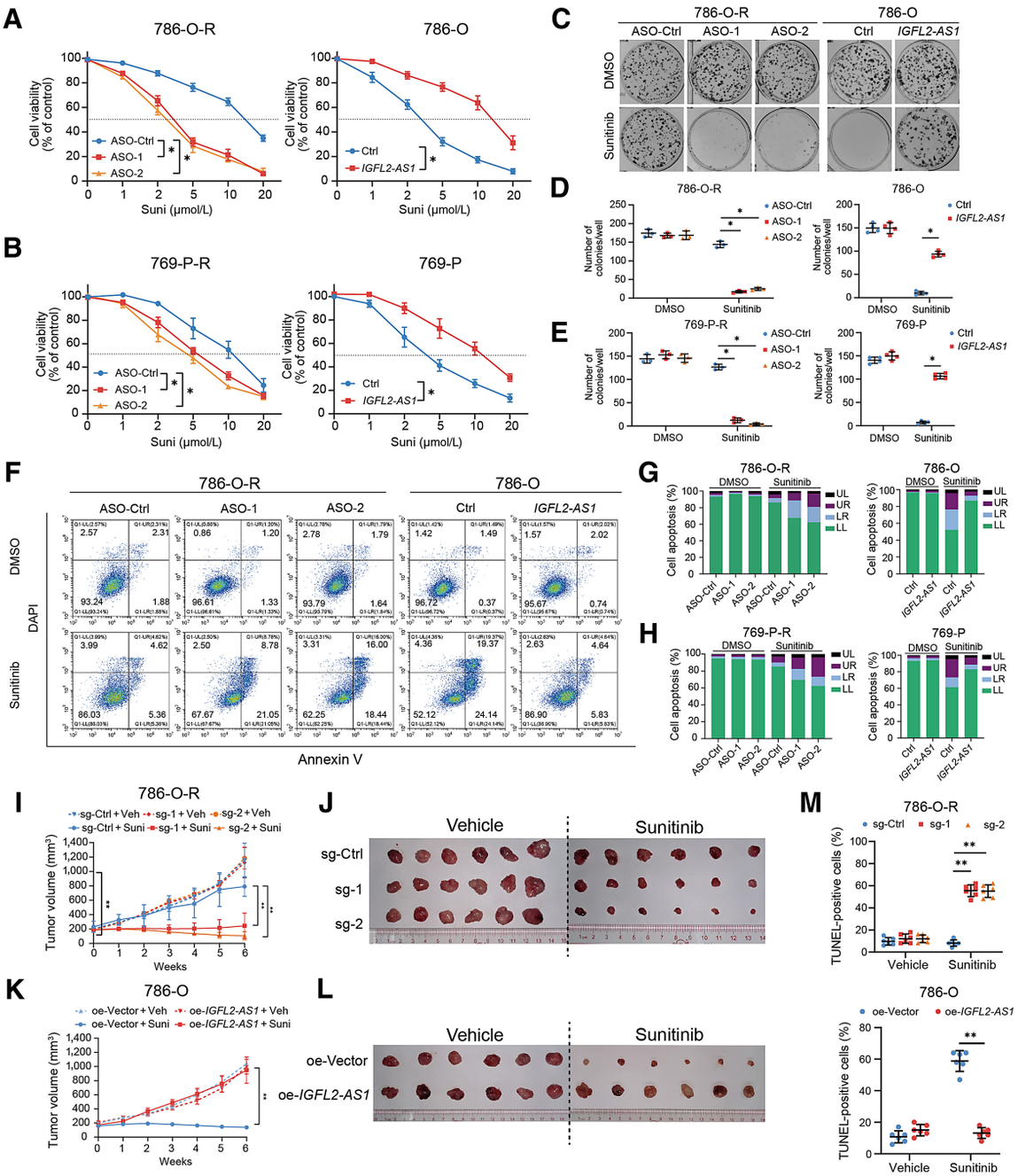

Figure 2.

IGFL2-AS1 promotes sunitinib resistance of RCC cells *in vitro* and *in vivo*. **A** and **B,** *IGFL2-AS1*-knockdown, *IGFL2-AS1*-overexpressing, and corresponding control cells were treated with the indicated concentrations of sunitinib for 60 hours ($n = 4$). **C–E,** Colony formation assay of *IGFL2-AS1*-knockdown, *IGFL2-AS1*-overexpressing, and corresponding control cells with sunitinib treatment (2 μmol/L) in 6-well dishes (500 cells per well) for 10 days ($n = 4$). **F–H,** Apoptosis analysis of *IGFL2-AS1*-knockdown, *IGFL2-AS1*-overexpressing, and corresponding control cells treated with sunitinib (2 μmol/L) for 60 hours. Stacked histograms showing the apoptosis distributions. UL, top left; UR, top right; LR, bottom right; LL, bottom left. **I** and **J,** Weekly measurements of tumor growth in *IGFL2-AS1*-knockdown and control cells. Representative images of tumors are shown ($n = 6$). **K** and **L,** Weekly measurements of tumor growth in *IGFL2-AS1*-overexpressing and control cells. Representative images of tumors are shown ($n = 6$). **M,** TUNEL assay showing apoptosis in the tumor. Data are shown as mean ± SD (error bars). *, $P < 0.05$; **, $P < 0.01$.

was positively correlated with *IGFL2-AS1* expression in tumor tissues of ccRCC patients (**Fig. 3E**). We therefore focused on the regulation of TP53INP2 by *IGFL2-AS1*. *TP53INP2* has five exons and four transcripts (splice variants; **Fig. 3F**). We first examined expression of 4 transcripts and confirmed two main transcripts, *TP53INP2*–001 and *TP53INP2*–003 (**Fig. 3G**; Supplementary Fig. S4C). *TP53INP2*–001 contains exon 2 (Incl. Exon2) and *TP53INP2*–003 skips exon 2 (Skip Exon2). Both transcripts contained the same coding sequence.

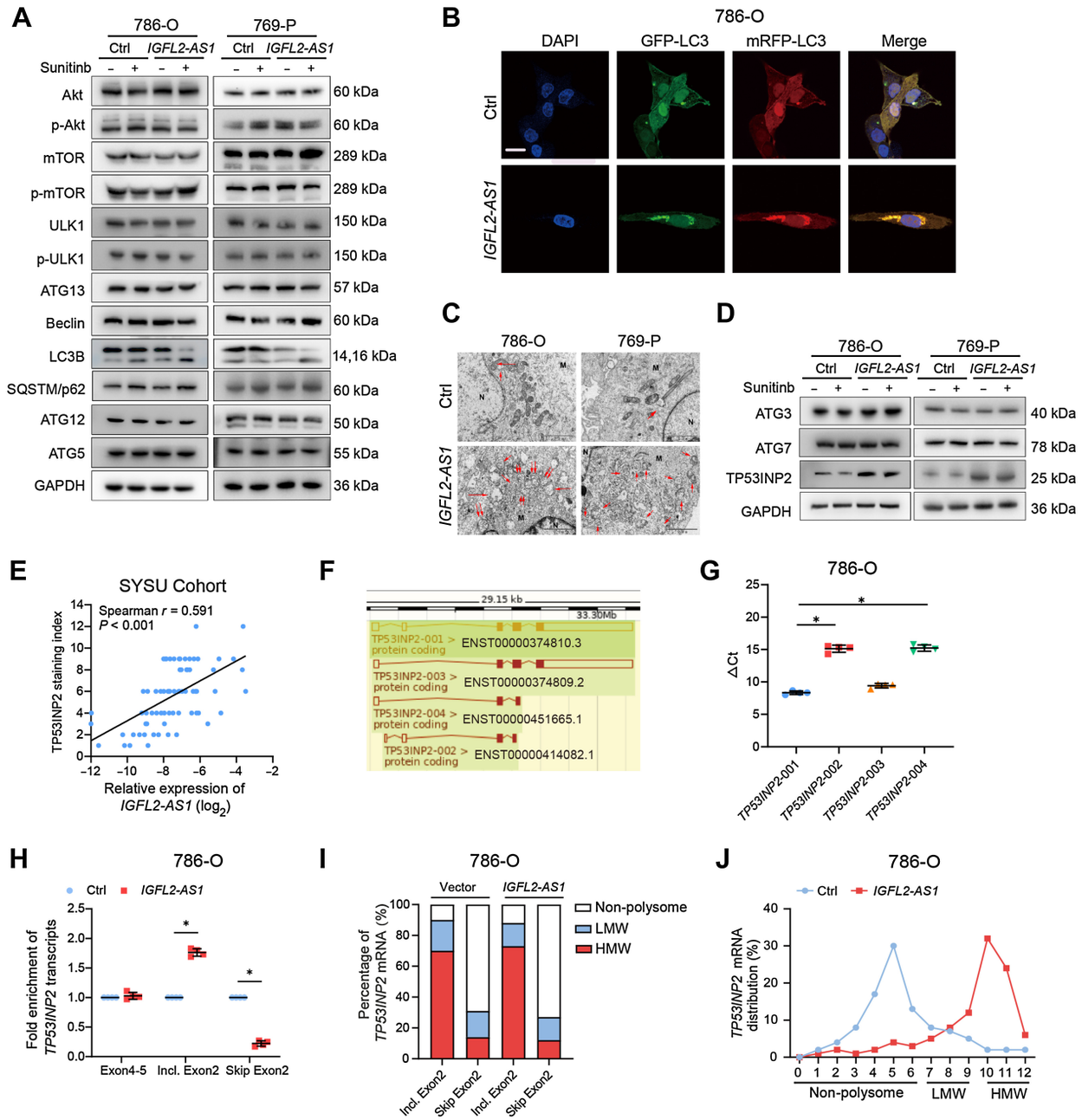

Figure 3.

IGFL2-AS1 overexpression enhances autophagy in RCC cells by regulating alternative splicing of *TP53INP2*. **A,** Western blotting analyses of autophagy pathway in the absence (−) or presence (+) of sunitinib (2 μmol/L) for 60 hours. **B,** Confocal microscopy showing autophagic flux in 786-O cells treated with sunitinib (2 μmol/L) for 60 hours. Scale bar, 20 μm. **C,** Electron micrographs indicating increased numbers of autophagosomes/autolysosomes (red arrows) in RCC cells treated with sunitinib (2 μmol/L) for 60 hours. **D,** Western blotting analyses of key regulators affecting the transition from LC3-I to LC3-II in the absence (−) or presence (+) of sunitinib (2 μmol/L) for 60 hours. **E,** Correlation analysis between *IGFL2-AS1* expression and TP53INP2 protein levels in the SYSU cohort. Tissue expressions of *IGFL2-AS1* were detected by qRT-PCR. Tissue protein levels of TP53INP2 were examined by IHC staining. **F,** The schematic diagram of four transcripts of *TP53INP2*. **G,** Validation of four transcripts of *TP53INP2* by qRT-PCR ($n = 4$). **H,** Validation of *TP53INP2* alternative splicing after *IGFL2-AS1* overexpression by qRT-PCR($n = 4$). **I** and **J,** Polysome profiles of 786-O cells after *IGFL2-AS1* overexpression. **I,** Distribution differences between Incl. Exon2 and Skip Exon2 transcripts in the sucrose gradient fractions. **J,** Relative distribution of total *TP53INP2* mRNA in the sucrose gradient fractions. Data are shown as mean ± SD (error bars). *, $P < 0.05$.

Interestingly, after overexpression of *IGFL2-AS1*, we observed increased levels of *TP53INP2* Incl. Exon2, and correspondingly reduced levels of *TP53INP2* Skip Exon2 (**Fig. 3H**; Supplementary Fig. S4D). However, there were no significant differences in the total levels of two *TP53INP2* transcripts. At the same time, we became aware that Jones and colleagues had also reported that alternative splicing (AS) of *TP53INP2* might affect cell function (26). Therefore, we decided to further investigate *IGFL2-AS1*-induced alternative splicing of *TP53INP2*. Generally speaking, mRNAs that distribute to the high molecular weight (HMW) polysomes possess higher translational efficiency than those distributing to the nonpolysomal fraction or low molecular weight (LMW) polysomes. Therefore, we performed polysome profile analysis. Notably, *TP53INP2* Incl. Exon2 was mainly located in the HMW, whereas *TP53INP2* Skip Exon2 mainly located in the non- and LMW polysomal fractions (**Fig. 3I**; Supplementary Figs. S4E–S4G). Correspondingly, overexpression of *IGFL2-AS1* significantly increased the proportion of total *TP53INP2* mRNAs in HMW polysomes (**Fig. 3J**; Supplementary Fig. S4H). These findings suggested that *IGFL2-AS1* might promote *TP53INP2* mRNA transcription efficiency via AS events.

IGFL2-AS1 functions by interacting with hnPNPC protein

To further explore how *IGFL2-AS1* upregulated TP53INP2, we first performed an RNA pulldown assay. Silver staining showed an overtly differential band, which was identified by MS as hnRNPC (**Fig. 4A** and **B**). hnRNPC belongs to the subfamily of hnRNP, which are RNA-binding proteins that play a role in precursor mRNA (pre-mRNA) processing, RNA nuclear export, m^6A regulation, among other functions (27, 28). Western blotting also confirmed the binding of *IGFL2-AS1* to hnRNPC (Supplementary Fig. S5A). Furthermore, RIP assay verified enrichment of *IGFL2-AS1* in hnRNPC precipitates (**Fig. 4C**). Confocal microscopy of *IGFL2-AS1* and hnRNPC immunostaining showed that *IGFL2-AS1* and hnRNPC mainly colocalized in and around the nucleus of RCC cells (**Fig. 4D**). Consistently, we found that *IGFL2-AS1* interacted with hnRNPC via RNA electrophoretic mobility shift assays (RNA EMSA; **Fig. 4E**). To confirm the specific binding motif of *IGFL2-AS1* to hnRNPC, we designed a series of *IGFL2-AS1* truncations. Deletion analysis revealed that the 120–160 nt region of *IGFL2-AS1* was essential for direct interaction with hnRNPC (**Fig. 4F** and **G**). To further identify the specific motif responsible for hnRNPC binding, we performed sequence analysis using the POSTAR2 database (**Fig. 4H**). The predicted binding sequence "CNGG" (N = G, A, T, or C) was also located in the 120–160 nt region of *IGFL2-AS1*, which is a stem-loop structure (**Fig. 4I**). After deleting the 120–160 nt fragment, *IGFL2-AS1* could no longer interact with hnRNPC (**Fig. 4J**; Supplementary Fig. S5B). After deleting the only one RNA recognition motif (RRM; 16–87 aa) region in hnRNPC, *IGFL2-AS1* could no longer interact with hnRNPC, indicating that the RRM of hnRNPC was the binding site for *IGFL2-AS1* (**Fig. 4K**; Supplementary Figs. S5C and S5D).

IGFL2-AS1 regulates alternative splicing of *TP53INP2* by competitively binding to hnRNPC

A previous study reported that the hnRNP family could regulate AS of *TP53INP2* mRNA (26), and so we examined the effect of hnRNPC on *TP53INP2* AS events. RIP assays showed that the RRM of hnRNPC was critical for the interaction with *TP53INP2* pre-mRNA (**Fig. 5A**). We further silenced hnRNPC in 786-O cells, and observed a decreased level of *TP53INP2* Skip Exon2 with a corresponding increase in levels of *TP53INP2* Incl. Exon2 (**Fig. 5B**; Supplementary Fig. S6A). Polysome profile analysis also showed enrichment of *TP53INP2* mRNAs in HMW when silencing hnRNPC (**Fig. 5C**; Supplementary Fig. S6B). The above results showed that the RRM region of hnRNPC could interact with *IGFL2-AS1* and *TP53INP2* pre-mRNA, and that both *IGFL2-AS1* and hnRNPC regulated *TP53INP2* AS events. We thus speculated about whether *IGFL2-AS1* could competitively bind to hnRNPC and sequester hnRNPC from *TP53INP2* pre-mRNA. Intriguingly, RIP assays showed that *IGFL2-AS1* overexpression notably inhibited the interaction of hnRNPC with *TP53INP2* pre-mRNA (**Fig. 5D**). However, this effect was attenuated when the 120–160 nt region of *IGFL2-AS1* was deleted. Furthermore, after silencing hnRNPC, *IGFL2-AS1* knockdown could not regulate AS events and the mRNA distribution of *TP53INP2* (**Fig. 5E** and **F**; Supplementary Fig. S6C). Meanwhile, the effect of *IGFL2-AS1* knockdown on autophagy-induced sunitinib resistance was largely abolished upon hnRNPC knockdown (Supplementary Fig. S6D).

To reverse the sunitinib-resistant effect of *IGFL2-AS1*, we stably silenced *TP53INP2* in control and *IGFL2-AS1* overexpressing cells (**Fig. 5G**). The high ratio of LC3-II/LC3-I caused by *IGFL2-AS1* overexpression was reversed by *TP53INP2* knockdown. Moreover, *TP53INP2* knockdown rescued sunitinib-resistant effect of *IGFL2-AS1* on RCC cells *in vitro* and *in vivo* (**Fig. 5H** and **I**; Supplementary Figs. S6E–S6J). All these findings indicated that *IGFL2-AS1* positively regulated *TP53INP2* translation efficiency by competitively binding to hnRNPC, and conversely *TP53INP2* knockdown attenuated the sunitinib-resistant effect of *IGFL2-AS1*.

hnRNPC mediates *IGFL2-AS1* packaging into EVs

A growing body of evidence has demonstrated that ncRNA are enriched in EVs. Therefore, we examined EV-packaged *IGFL2-AS1* in the sera of patients with ccRCC and culture media (CM) of RCC cells. We first validated the characteristics of the particles isolated from the sera and CM (Supplementary Figs. S7A–S7F). Kaplan–Meier survival analysis showed poorer survival outcome in the high expression group (**Fig. 6A**; Supplementary Fig. S7G; Supplementary Tables S3 and S4), indicating that EV-packaged *IGFL2-AS1* might play an important role in the transmission of sunitinib resistance. The expression pattern of EV-packaged *IGFL2-AS1* was similar to that of cellular *IGFL2-AS1*, suggesting that EV-packaged *IGFL2-AS1* could also function in sunitinib resistance (Supplementary Figs. S7H and S7I).

Recently, hnRNPC has been reported to control sorting of ncRNAs into EVs by binding to EXOmotifs (GGAG/CCCU; refs. 27, 29). The Vesiclepedia database also showed abundant hnRNPC in EVs (Supplementary Fig. S7J). Intriguingly, we found several EXOmotifs in the binding region of *IGFL2-AS1* to hnRNPC, so we suspected that hnRNPC might guide *IGFL2-AS1* into EVs. We performed qRT-PCR analysis and found that silencing of hnRNPC could inhibit loading of *IGFL2-AS1* into EVs (**Fig. 6B**). Meanwhile, truncated IGFLA-AS1 could not be enriched in EVs, which indicated that the 120–160 nt region is important for *IGFL2-AS1* packaging into EVs (**Fig. 6C**).

IGFL2-AS1 transmits sunitinib resistance via EVs

To determine whether *IGFL2-AS1* could transmit sunitinib resistance to the sensitive cells, we first confirmed internalization of EVs (**Fig. 6D** and **E**). Compared with EVs isolated from control CM, EVs isolated from CM of *IGFL2-AS1* knockdown cells had no influence on *IGFL2-AS1* expression and cell viability of recipient cells (**Fig. 6F** and **G**). To further verify the effect of EV-packaged *IGFL2-AS1* on sunitinib resistance, we established an *in vivo* tumor model (**Fig. 6H**). Intriguingly, 2 weeks after treatment, tumor growth, size, and weight in the group injected with EV-786-$O_{oe\text{-}IGFL2\text{-}AS1}$ were significantly

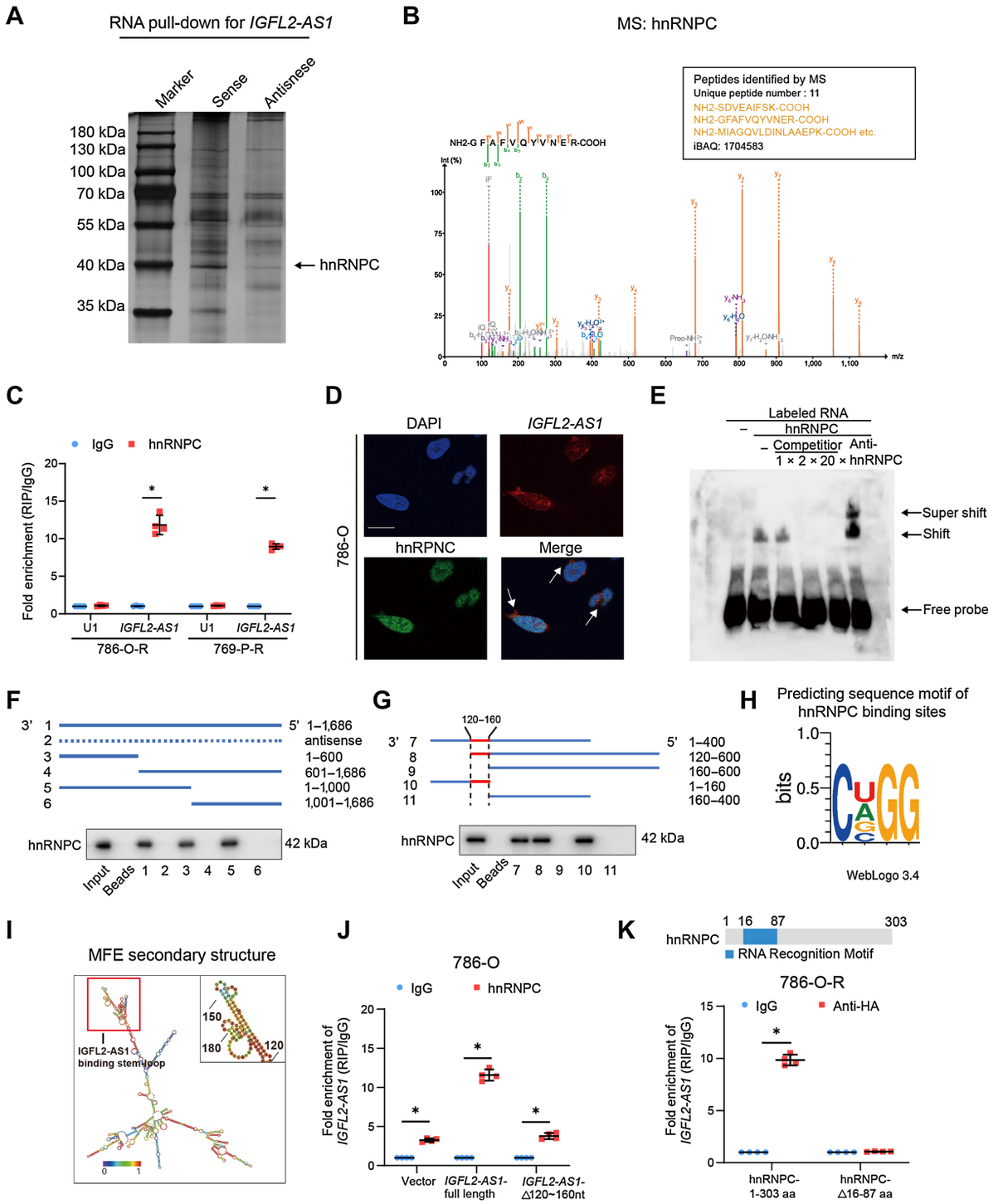

Figure 4.

IGFL2-AS1 functions by binding to hnPNPC protein. **A,** RNA pulldown assay with full-length and antisense RNAs in 786-O cells, followed by silver staining. **B,** MS of *IGFL2-AS1* binding proteins. **C,** RIP with control IgG and anti-hnRNPC antibodies to examine the enrichment of *IGFL2-AS1* in sunitinib-resistant RCC cells ($n = 4$). **D,** Confocal microscopy of *IGFL2-AS1* and hnRNPC immunostaining. White arrow, colocalization around the nucleus. Scale bar, 10 μm. **E,** RNA EMSA assay showing binding of biotin-labeled *IGFL2-AS1* and purified hnRNPC. **F** and **G,** A series of deletion analyses of *IGFL2-AS1* via RNA pulldown assays. **H,** Predicted binding sequence motif of *IGFL2-AS1* using the POSTAR2 database. **I,** Predicted minimal folding free energy secondary structures of *IGFL2-AS1* (RNAfold web server). **J,** RIP assays after overexpression of truncated *IGFL2-AS1* in 786-O ($n = 4$). **K,** Top, schematic diagram of hnRNPC RRM; bottom, RIP assays after overexpression of truncated hnRNPC ($n = 4$). Data are shown as mean ± SD (error bars). *, $P < 0.05$.

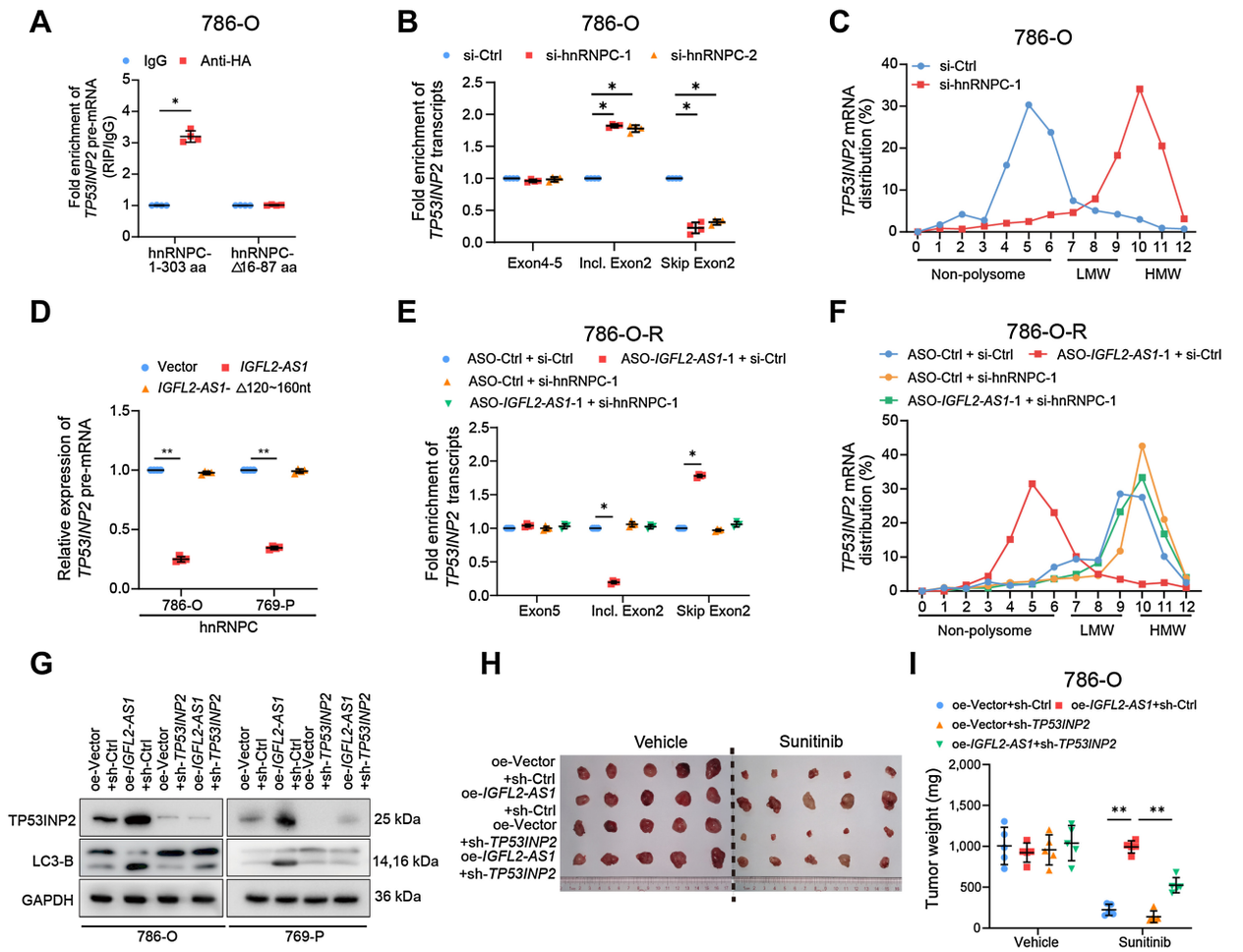

Figure 5.

IGFL2-AS1 regulates alternative splicing of *TP53INP2* through competitively binding to hnRNPC. **A,** RIP assays after overexpression of full-length and truncated hnRNPC in 786-O cells revealed hnRNPC binding to *TP53INP2* pre-mRNA, and the RRM region of hnRNPC was crucial for this interaction ($n = 4$). **B,** Validation of *TP53INP2* alternative splicing after silencing hnRNPC by qRT-PCR ($n = 4$). **C,** Polysome profile analyses of 786-O cells after silencing of hnRNPC. **D,** RIP assay after overexpression of truncated *IGFL2-AS1* revealing that *IGFL2-AS1* might regulate AS of *TP53INP2* through competitive binding of hnRNPC ($n = 4$). **E** and **F,** Silencing of hnRNPC suppressed regulation of *TP53INP2* AS by *IGFL2-AS1* ($n = 4$). **G,** Western blotting analysis showing decreased expression levels of *TP53INP2* and the reverse transition from LC3-II to LC3-I in the *IGFL2-AS1*-overexpressing *TP53INP2*-knockdown group in RCC cells treated with sunitinib (2 μmol/L) for 60 hours. **H,** Representative images of tumors are shown ($n = 5$). **I,** Tumor weight measured after surgical dissection. Data are shown as mean ± SD (error bars). *, $P < 0.05$; **, $P < 0.01$.

increased compared with the control groups (**Fig. 6I** and **J**; Supplementary Fig. S7K). Furthermore, a lower proportion of TUNEL-positive cells and higher expression levels of TP53INP2 were observed in the EV-786-$O_{oe\text{-}IGFL2\text{-}AS1}$ group (**Fig. 6K**). In conclusion, these data are consistent with an important role for EV-packaged *IGFL2-AS1* in the transmission of sunitinib resistance.

M^6A modification is critical to *IGFL2-AS1* interaction with hnRNPC

One of the most abundant internal modification sites in eukaryotic RNA is m^6A, which has been reported to alter local structure in mRNA and lncRNA to facilitate binding of hnRNPC (28). To identify whether m^6A is involved in the interaction of *IGFL2-AS1* with hnRNPC, we first examined m^6A levels in RCC cells treated with sunitinib. Intriguingly, we observed that m^6A levels were unchanged in 786-O-R cells, indicating stable m^6A modification in sunitinib-resistant RCC cells treated with sunitinib (Supplementary Fig. S8A). We next examined all the predicted m^6A modified sites in *IGFL2-AS1* and also found m^6A modification in the 120–160 nt region of *IGFL2-AS1* (Supplementary Fig. S8B and S8C). m^6A -IP-qPCR (meRIP-qPCR) analysis showed that *IGFL2-AS1* was enriched in m^6A antibody precipitates (Supplementary Fig. S8D). It is already known that METTL3 (N6-adenosine-methyltransferase) and ALKBH5 (RNA demethylase) play an important role in m^6A modification (30). MeRIP-qPCR performed after MELLT3 overexpression and ALKBH5 overexpression revealed that *IGFL2-AS1* could be regulated by m^6A modification in RCC cells (Supplementary Figs. S8E–S8G). Meanwhile, we performed an RIP assay and found that *IGFL2-AS1* was enriched in hnRNPC precipitates after MELLT3 overexpression (Supplementary Fig. S8H). Conversely, we found less *IGFL2-AS1* in hnRNPC precipitates after ALKBH5 overexpression. Furthermore, overexpression of *IGFL2-AS1* with a mutated GGACT motif, the predicted modified

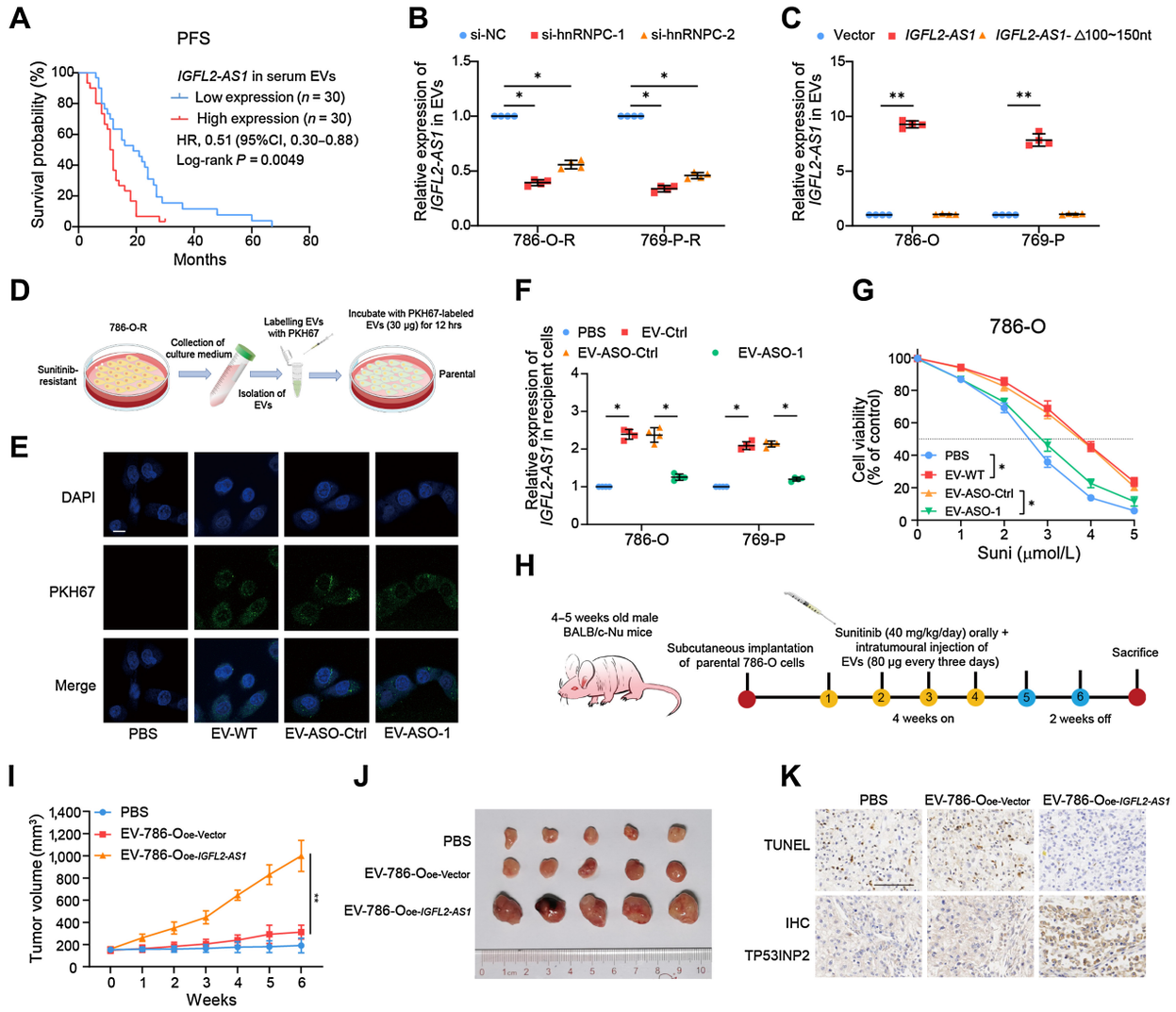

Figure 6.

hnRNPC mediates *IGFL2-AS1* packaging into EVs and transmission of sunitinib resistance. **A,** Kaplan–Meier survival analysis showing poorer PFS in the high serumal *IGFL2-AS1* expression group. **B,** qRT-PCR analysis of EV-packaged *IGFL2-AS1* expression released by hnRNPC knockdown RCC cells ($n = 4$). **C,** qRT-PCR analysis of EV-packaged *IGFL2-AS1* expression released by cells overexpressing truncated *IGFL2-AS1* ($n = 4$). **D,** Schematic diagram of EV labeling and internalization. **E,** Representative confocal images of internalized EVs labeled with PKH-67. Scale bar, 20 μm. **F,** qRT-PCR analysis of *IGFL2-AS1* expression 60 hours after incubation with indicated EVs or PBS ($n = 4$). **G,** RCC cells incubated with EVs isolated from *IGFL2-AS1* knockdown and corresponding control CM at the indicated concentrations of sunitinib (2 μmol/L) for 60 hours ($n = 4$). **H,** Schematic illustration of the establishment of the *in vivo* tumor model. **I,** Weekly measurements of tumor growth ($n = 5$). **J,** Representative images of tumors are shown. **K,** Representative images of the TUNEL assay and IHC. Scale bar, 100 μm. Data are shown as mean ± SD (error bars). *, $P < 0.05$; **, $P < 0.01$.

m^{6}A site in the 120–160 nt region, showed attenuated *IGFL2-AS1* interaction with hnRNPC (Supplementary Figs. S8I and S8J). MELLT3 overexpression could partially rescue impaired cell viability caused by mutated *IGFL2-AS1* in RCC cells (Supplementary Fig. S8K). All the results above indicated that m^{6}A modification was critical to *IGFL2-AS1* interaction with hnRNPC.

Nanomedicine consisting of C-SLN/ASO-*IGFL2-AS1* complexes recovers sunitinib sensitivity *in vivo*

For the complexation and delivery of ASO-*IGFL2-AS1* to cells *in vivo*, we designed an effective and safe C-SLNs carrier (**Fig. 7A**). C-SLNs had an average particle size of 247 ± 27 nm (Supplementary Fig. S9A). The mean zeta potential of chitosan-SLNs was 1.4 ± 0.3 mV at near-neutral pH. A TEM image of chitosan-SLNs indicated successful adsorption of chitosan onto the surface of SLNs (Supplementary Fig. S9B). ASO binding assay showed that C-SLNs mixed with ASOs at a mass ratio of 1:1.5 or higher were nearly invisible, indicating strong binding of C-SLN complexes (Supplementary Fig. S9C). The low cytotoxicity and high transfection efficiency of C-SLNs suggest that they are a promising nanocarrier of ASO-drugs (Supplementary Figs. S9D–S9F).

To apply C-SLN/ASO complexes *in vivo*, we constructed seven ccRCC PDX models (Supplementary Table S5). PDX5, which had the highest expression level of *IGFL2-AS1* in tumor tissue and highest IC_{50}

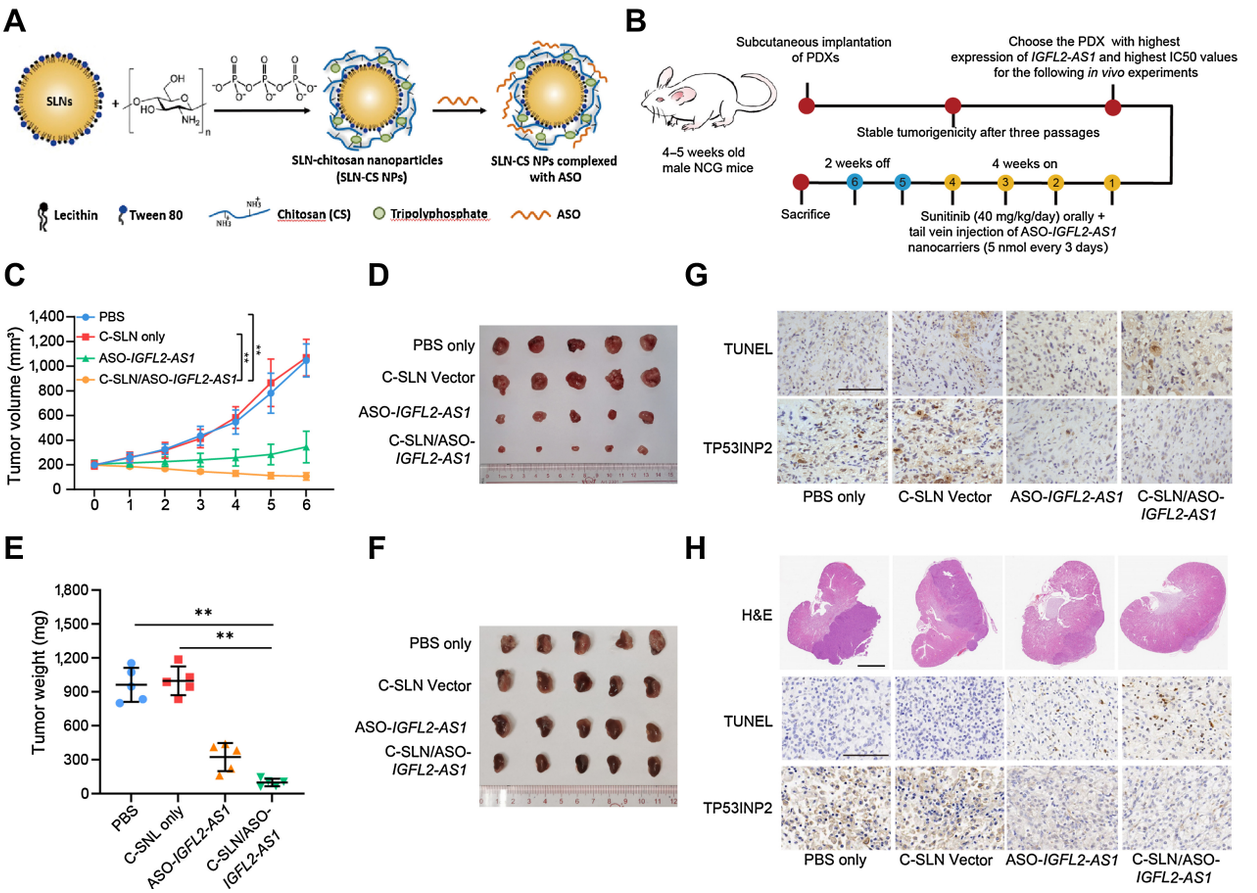

Figure 7.

Characteristics of C-SLN nanoparticles and *in vivo* application of C-SLN/ASO-*IGFL2-AS1* complexes. **A,** Chemical structure of chitosan molecules and schematic illustration of C-SLN nanoparticle formation. **B,** Schematic illustration showing the establishment of RCC PDX models and tail vein injection of nanodrugs. **C,** Weekly measurements of tumor growth in NCG mice injected with nanodrugs and treated with sunitinib ($n = 5$). **D,** Representative images of subcutaneous tumors. **E,** Tumor weight of subcutaneous tumors was measured after surgical resection. **F,** Representative images of orthotopic tumors ($n = 5$). **G** and **H,** Representative images of hematoxylin and eosin (H&E), TUNEL assay, and IHC. Scale bar for H&E, 2.5 mm. Scale bar for TUNEL and IHC, 100 μm. Data are shown as mean ± SD (error bars). **, $P < 0.01$.

value of sunitinib among all the PDXs, was used for ASO nanodrugs (Supplementary Figs. S9G–S9I;). The fluorescence images after tail vein injection of nanodrugs showed that C-SLN/FAM-ASO-*IGFL2-AS1* was stable in the circulation and could be specifically delivered to tumors *in vivo* (Supplementary Fig. S9J).

Furthermore, we used an orthotopic model and a subcutaneous model, respectively, to examined the potency of C-SLN/ASO-*IGFL2-AS1 in vivo* (**Fig. 7B**). Notably, the C-SLN/ASO-*IGFL2-AS1* group achieved the best therapeutic effects, suggesting recovery of sunitinib sensitivity *in vivo* (**Fig. 7C–F**). A higher proportion of TUNEL positive cells and reduced expression of TP53INP2 were also observed in the C-SLN/ASO-*IGFL2-AS1* group (**Fig. 7G** and **H**). To sum up, our nanomedicine consisting of C-SLN/ASO-*IGFL2-AS1* complexes could recover sunitinib sensitivity *in vivo*.

Extended applicability of *IGFL2-AS1* to resistance of cabozantinib and axitinib in RCC cells

Treatment options for patients with mccRCC have dramatically increased. Contemporary targeted treatments like cabozantinib and axitinib have a priority in the combined treatment of mccRCC (31, 32). Because sunitinib, cabozantinib, and axitinib all belong to TKIs, we wonder whether the sunitinib-resistant effect of *IGFL2-AS1* could be extended to cabozantinib and axitinib. Surprisingly, *IGFL2-AS1* overexpression also resulted in increased cell viability in RCC cells treated with cabozantinib or axitinib (Supplementary Figs. S10A and S10B). Meanwhile, decreased apoptosis was observed in IGFL2-AS-overexpression group when treated with cabozantinib or axitinib (Supplementary Figs. S10C and S10D). Moreover, confocal microscopy of labeled LC3 also showed enhanced autophagy in *IGFL2-AS1*-overexpressing RCC cells upon cabozantinib or axitinib treatment (Supplementary Figs. S10E and S10F). These results indicated that *IGFL2-AS1* might trigger cabozantinib and axitinib resistance in RCC by enhancing autophagy as well.

Discussion

Sunitinib has been recommended for the treatment of mccRCC over 10 years. However, the mechanisms of inherent and acquired sunitinib resistance remain unclear. In this study, we first identified a novel lncRNA-*IGFL2-AS1* in two acquired sunitinib-resistant RCC models. Specifically, *IGFL2-AS1* regulated alternative splicing of *TP53INP2* mRNA via competitively binding to hnRNPC, which enhanced

autophagy and further facilitated sunitinib resistance. Moreover, *IGFL2-AS1* could be packaged into EVs via binding to hnRNPC to transmit sunitinib resistance to sensitive RCC cells. Finally, we developed a novel nano-carrier, C-SLN, which could deliver ASO-*IGFL2-AS1* stably and efficiently via intravenous injection. Besides, we also explored extended applicability of *IGFL2-AS1* to resistance of cabozantinib and axitinib in RCC cells. These results indicate that *IGFL2-AS1* potentially can be a prognostic indicator for mccRCC and serve as a therapeutic target in sunitinib treatment.

Recently, a growing number of studies have reported that lncRNAs facilitate chemoresistance through activation of autophagy (33, 34). However, the roles lncRNAs play in targeted drug resistance through autophagy are unknown. Giuliano and colleagues once reported that enhanced autophagy accelerated the formation of autolysosome formation and then promoted sunitinib resistance via its sequestration, indicating a critical role for autophagy in sunitinib resistance (35). TP53INP2 has been characterized as a key player in transcription and autophagy (36). In the presence of stress, TP53INP2 recruits LC3 family proteins to the cytoplasm and facilitates the autophagosome biogenesis (37, 38). Jones and colleagues found that hnRNPA2 knockdown increased *TP53INP2* exon 2 skipping transcripts, and thus inhibited invasive migration of tumor cells (26). However, the underlying mechanism of the different *TP53INP2* mRNA transcripts remained unexplained. Herein, we also observed alternative splicing of *TP53INP2* mRNA caused by interaction between *IGFL2-AS1* and hnRNPC. In consideration of changes in the TP53INP2 protein rather than *TP53INP2* mRNA, we used polysome analysis to demonstrate that *TP53INP2* exon 2 inclusive transcripts had a higher translation efficiency. This finding revealed a novel mechanism of TP53INP2 regulation by *IGFL2-AS1* in sunitinib-resistant RCC cells.

Recent studies have shown that ncRNA can be selectively sorted to EVs by membrane or RNA-binding proteins (27, 39–41). For example, Beltri and colleagues found that hnRNPA2B1, hnRNPA1 and hnRNPC could specifically bind the EXOmotifs GGAG/CCCU, and direct miRNAs to EVs (27). Moreover, these EXOmotifs could also guide the load of lncRNAs to EVs (18, 19). Herein, we found several EXOmotifs in the 120–160 nt region of *IGFL2-AS1* and demonstrated that *IGFL2-AS1* can be guided to EVs by interaction with hnRNPC. However, more investigations are needed to understand the mechanisms of hnRNPC shuttling from the nucleus to the EVs in the cytoplasm.

A limitation of our study is that, with the rapid development of therapies, combinations of TKIs and immune checkpoint inhibitors have become the preferred regimens in ccRCC. Nonetheless, sunitinib is still one of the most representative targeted drugs. Our findings could also contribute to the understanding of resistance to cabozantinib and axitinib in ccRCC. Second, sunitinib-resistant RCC cell lines could not directly reflect the biology seen in human on treatment. Ideally identification of sunitinib-resistant-related biomarkers would come from human PDX models.

Authors' Disclosures

No author disclosures were reported.

Authors' Contributions

Y. Pan: Conceptualization, data curation, formal analysis, validation, investigation, visualization, methodology, writing–original draft, writing–review and editing. **X. Lu:** Conceptualization, data curation, software, formal analysis, validation, visualization, methodology, writing–original draft. **G. Shu:** Conceptualization, software, validation, visualization. **J. Cen:** Conceptualization, data curation, formal analysis, funding acquisition, validation, writing–review and editing. **J. Lu:** Conceptualization, funding acquisition, validation, investigation, writing–review and editing. **M. Zhou:** Validation, visualization. **K. Huang:** Resources, software. **J. Dong:** Validation, investigation. **J. Li:** Conceptualization, resources. **H. Lin:** Validation, investigation. **H. Song:** Validation, investigation. **Q. Xu:** Validation, investigation. **H. Han:** Resources, data curation, project administration, writing–review and editing. **Z. Chen:** Conceptualization, resources, funding acquisition, writing–review and editing. **W. Chen:** Conceptualization, resources, funding acquisition, writing–review and editing. **J. Luo:** Conceptualization, resources, supervision, funding acquisition, project administration, writing–review and editing. **J. Wei:** Conceptualization, resources, supervision, funding acquisition, writing–original draft, writing–review and editing. **J. Zhang:** Conceptualization, resources, supervision, funding acquisition, project administration, writing–review and editing.

Acknowledgments

The authors thank Zhicheng Xiang (SYSUCC) for technical assistance. This work was supported by National Natural Science Foundation of China (81772514, 82073381, 81725016, 81872094, 81602219, 81772718, 82002684, 81902576), Pearl River S&T Nova Program of Guangzhou (201806010005), the Natural Science Foundation of Guangdong (Nos. S2019B151502046 and 201704020174), and China Postdoctoral Science Foundation Funded Project (Nos. 236464, 2021TQ0381, and 2021M703700).

The publication costs of this article were defrayed in part by the payment of publication fees. Therefore, and solely to indicate this fact, this article is hereby marked "advertisement" in accordance with 18 USC section 1734.

Note

Supplementary data for this article are available at Cancer Research Online (http://cancerres.aacrjournals.org/).

Received October 16, 2021; revised January 24, 2022; accepted October 12, 2022; published first October 20, 2022.

References

1. Siegel RL, Miller KD, Fuchs HE, Jemal A. Cancer statistics, 2021. CA Cancer J Clin 2021;71:7–33.
2. Lipworth L, Morgans AK, Edwards TL, Barocas DA, Chang SS, Herrell SD, et al. Renal cell cancer histological subtype distribution differs by race and sex. BJU Int 2016;117:260–5.
3. Choueiri TK, Motzer RJ. Systemic therapy for metastatic renal-cell carcinoma. N Engl J Med 2017;376:354–66.
4. Barata PC, Rini BI. Treatment of renal cell carcinoma: current status and future directions. CA Cancer J Clin 2017;67:507–24.
5. Chow LQ, Eckhardt SG. Sunitinib: from rational design to clinical efficacy. J Clin Oncol 2007;25:884–96.
6. Motzer RJ, Hutson TE, Tomczak P, Michaelson MD, Bukowski RM, Oudard S, et al. Overall survival and updated results for sunitinib compared with interferon alfa in patients with metastatic renal cell carcinoma. J Clin Oncol 2009;27:3584–90.
7. Rini BI, Michaelson MD, Rosenberg JE, Bukowski RM, Sosman JA, Stadler WM, et al. Antitumor activity and biomarker analysis of sunitinib in patients with bevacizumab-refractory metastatic renal cell carcinoma. J Clin Oncol 2008;26:3743–8.
8. Sato T, Kawasaki Y, Maekawa M, Takasaki S, Morozumi K, Sato M, et al. Metabolomic analysis to elucidate mechanisms of sunitinib resistance in renal cell carcinoma. Metabolites 2020;11:1.
9. White E. Deconvoluting the context-dependent role for autophagy in cancer. Nat Rev Cancer 2012;12:401–10.
10. Mele L, la Noce M, Paino F, Regad T, Wagner S, Liccardo D, et al. Glucose-6-phosphate dehydrogenase blockade potentiates tyrosine kinase inhibitor effect on breast cancer cells through autophagy perturbation. J Exp Clin Cancer Res 2019;38:160.
11. Mele L, Del Vecchio V, Liccardo D, Prisco C, Schwerdtfeger M, Robinson N, et al. The role of autophagy in resistance to targeted therapies. Cancer Treat Rev 2020;88:102043.
12. Lee H, Zhang Z, Krause HM. Long noncoding RNAs and repetitive elements: junk or intimate evolutionary partners? Trends Genet 2019;35:892–902.

13. Statello L, Guo CJ, Chen LL, Huarte M. Gene regulation by long non-coding RNAs and its biological functions. Nat Rev Mol Cell Biol 2021;22:96–118.
14. Chen X, Xie R, Gu P, Huang M, Han J, Dong W, et al. Long noncoding RNA LBCS inhibits self-renewal and chemoresistance of bladder cancer stem cells through epigenetic silencing of SOX2. Clin Cancer Res 2019;25:1389–403.
15. Hua JT, Ahmed M, Guo H, Zhang Y, Chen S, Soares F, et al. Risk SNP-mediated promoter-enhancer switching drives prostate cancer through lncRNA PCAT19. Cell 2018;174:564–75.
16. Kim J, Piao HL, Kim BJ, Yao F, Han Z, Wang Y, et al. Long noncoding RNA MALAT1 suppresses breast cancer metastasis. Nat Genet 2018;50:1705–15.
17. Hu Q, Li C, Wang S, Li Y, Wen B, Zhang Y, et al. LncRNAs-directed PTEN enzymatic switch governs epithelial-mesenchymal transition. Cell Res 2019;29:286–304.
18. Qu L, Ding J, Chen C, Wu ZJ, Liu B, Gao Y, et al. Exosome-transmitted lncARSR promotes sunitinib resistance in renal cancer by acting as a competing endogenous RNA. Cancer Cell 2016;29:653–68.
19. Chen C, Luo Y, He W, Zhao Y, Kong Y, Liu H, et al. Exosomal long noncoding RNA LNMAT2 promotes lymphatic metastasis in bladder cancer. J Clin Invest 2020;130:404–21.
20. Volders PJ, Anckaert J, Verheggen K, Nuytens J, Martens L, Mestdagh P, et al. LNCipedia 5: towards a reference set of human long non-coding RNAs. Nucleic Acids Res 2019;47D1:D135–9.
21. Zhu Y, Xu G, Yang YT, Xu Z, Chen X, Shi B, et al. POSTAR2: deciphering the post-transcriptional regulatory logics. Nucleic Acids Res 2019;47:D203–11.
22. Zhou Y, Zeng P, Li YH, Zhang Z, Cui Q. SRAMP: prediction of mammalian N6-methyladenosine (m6A) sites based on sequence-derived features. Nucleic Acids Res 2016;44:e91.
23. Liu S, Zhu A, He C, Chen M. REPIC: a database for exploring the N(6)-methyladenosine methylome. Genome Biol 2020;21:100.
24. Pathan M, Fonseka P, Chitti SV, Kang T, Sanwlani R, Van Deun J, et al. Vesiclepedia 2019: a compendium of RNA, proteins, lipids and metabolites in extracellular vesicles. Nucleic Acids Res 2019;47:D516–9.
25. Gronwald J, Storkel S, Holtgreve-Grez H, Hadaczek P, Brinkschmidt C, Jauch A, et al. Comparison of DNA gains and losses in primary renal clear cell carcinomas and metastatic sites: importance of 1q and 3p copy number changes in metastatic events. Cancer Res 1997;57:481–7.
26. Moran-Jones K, Grindlay J, Jones M, Smith R, Norman JC. hnRNP A2 regulates alternative mRNA splicing of TP53INP2 to control invasive cell migration. Cancer Res 2009;69:9219–27.
27. Villarroya-Beltri C, Gutierrez-Vazquez C, Sanchez-Cabo F, Perez-Hernandez D, Vazquez J, Martin-Cofreces N, et al. Sumoylated hnRNPA2B1 controls the sorting of miRNAs into exosomes through binding to specific motifs. Nat Commun 2013;4:2980.
28. Liu N, Dai Q, Zheng G, He C, Parisien M, Pan T. N(6)-methyladenosine-dependent RNA structural switches regulate RNA-protein interactions. Nature 2015;518:560–4.
29. Balaguer N, Moreno I, Herrero M, Gonzalez M, Simon C, Vilella F. Heterogeneous nuclear ribonucleoprotein C1 may control miR-30d levels in endometrial exosomes affecting early embryo implantation. Mol Hum Reprod 2018;24:411–25.
30. Zaccara S, Ries RJ, Jaffrey SR. Reading, writing and erasing mRNA methylation. Nat Rev Mol Cell Biol 2019;20:608–24.
31. Choueiri TK, Powles T, Burotto M, Escudier B, Bourlon MT, Zurawski B, et al. Nivolumab plus cabozantinib versus sunitinib for advanced renal-cell carcinoma. N Engl J Med 2021;384:829–41.
32. Powles T, Plimack ER, Soulieres D, Waddell T, Stus V, Gafanov R, et al. Pembrolizumab plus axitinib versus sunitinib monotherapy as first-line treatment of advanced renal cell carcinoma (KEYNOTE-426): extended follow-up from a randomised, open-label, phase 3 trial. Lancet Oncol 2020;21:1563–73.
33. Zhang F, Wang H, Yu J, Yao X, Yang S, Li W, et al. LncRNA CRNDE attenuates chemoresistance in gastric cancer via SRSF6-regulated alternative splicing of PICALM. Mol Cancer 2021;20:6.
34. Luo Y, Zheng S, Wu Q, Wu J, Zhou R, Wang C, et al. Long noncoding RNA (lncRNA) EIF3J-DT induces chemoresistance of gastric cancer via autophagy activation. Autophagy 2021;1–19.
35. Giuliano S, Cormerais Y, Dufies M, Grepin R, Colosetti P, Belaid A, et al. Resistance to sunitinib in renal clear cell carcinoma results from sequestration in lysosomes and inhibition of the autophagic flux. Autophagy 2015;11:1891–904.
36. Xu Y, Wan W. The bifunctional role of TP53INP2 in transcription and autophagy. Autophagy 2020;16:1341–3.
37. Nowak J, Iovanna JL. TP53INP2 is the new guest at the table of self-eating. Autophagy 2009;5:383–4.
38. You Z, Xu Y, Wan W, Zhou L, Li J, Zhou T, et al. TP53INP2 contributes to autophagosome formation by promoting LC3-ATG7 interaction. Autophagy 2019;15:1309–21.
39. Arroyo JD, Chevillet JR, Kroh EM, Ruf IK, Pritchard CC, Gibson DF, et al. Argonaute2 complexes carry a population of circulating microRNAs independent of vesicles in human plasma. Proc Natl Acad Sci U S A 2011;108:5003–8.
40. Lee H, Li C, Zhang Y, Zhang D, Otterbein LE, Jin Y. Caveolin-1 selectively regulates microRNA sorting into microvesicles after noxious stimuli. J Exp Med 2019;216:2202–20.
41. Kosaka N, Iguchi H, Hagiwara K, Yoshioka Y, Takeshita F, Ochiya T. Neutral sphingomyelinase 2 (nSMase2)-dependent exosomal transfer of angiogenic microRNAs regulate cancer cell metastasis. J Biol Chem 2013;288:10849–59.